CrystEngComm

PAPER

View Article Online
View Journal | View Issue

Cite this: *CrystEngComm*, 2015, **17**, 4383

Crosslinking of the $Pd(acacCN)_2$ building unit with Ag(I) salts: dynamic 1D polymers and an extended 3D network†

Qianqian Guo,[a] Carina Merkens,[a] Runze Si[b] and Ulli Englert*[a]

Received 8th January 2015,
Accepted 5th May 2015

DOI: 10.1039/c5ce00043b

www.rsc.org/crystengcomm

After deprotonation, the acetylacetonate moiety of the ditopic ligand 3-cyanoacetylacetone (HacacCN) acts as a chelating ligand towards Pd(II). The resulting square-planar complex $Pd(acacCN)_2$ represents a suitable building unit for extended structures *via* coordination of Ag(I) cations to the peripheral nitrile groups. These target compounds have been structurally characterized: with silver salts of the anions BF_4^-, ClO_4^-, PF_6^- and $CF_3SO_3^-$, chain polymers with an alternating sequence of Pd(II) and Ag(I) are obtained. Solvent molecules and counter anions fill voids close to the silver cations; more weakly coordinating anions are engaged in longer, the triflate anion in a shorter interaction to Ag(I). In contrast to powder samples, larger crystals of these one-dimensional polymers are rather stable with respect to desolvation. Two isomorphous 1D structures undergo a fully reversible k_2 phase transition which can be monitored by single crystal diffraction. The phase transition temperature depends on the nature of the counter anion and may therefore be tuned as a function of chemical composition. The formation of chain polymers by linking $Pd(acacCN)_2$ building blocks with Ag(I) salts of BF_4^-, ClO_4^-, PF_6^- and $CF_3SO_3^-$ follows chemical intuition whereas its reaction with silver nitrate leads to an unexpected and close-packed 3D structure in which layers of composition $Ag(NO_3)$ are connected by $Pd(acacCN)_2$ linkers.

1 Introduction

The structural chemistry of coordination polymers has attracted wide interest over the last decades: many cations may act as potential coordination centers, and they can be interconnected by a wide range of electronically and geometrically different ligands. The resulting solids often show tunable[1,2] and useful properties, *e.g.* for applications in gas storage,[3–5] separation,[6] optics,[7] or magnetochemistry.[8]

Bimetallic coordination polymers, *i.e.* extended solids based on the regular arrangement of more than one type of cation, offer additional challenges for synthesis and potential for application. Among the linkers for such bimetallic systems, substituted acetylacetonates (acac) have been particularly successful. Two obvious reasons for this success shall shortly be mentioned: the chelating nature of the acetylacetonato moiety conveys additional stability to metal coordination by this group of the ditopic linker, and the different Pearson hardnesses[9] of the potential coordination sites favour crosslinking of different cations without disorder. Four examples of ditopic Hacac derivatives have been compiled in Scheme 1.

O,*O*′ coordination by the chelating acac moiety is possible in all these ligands. In addition, the pyridine derivatives in Scheme 1 (ligands a–c) behave as good N nucleophiles to metal cations. This was confirmed in reports about the coordination chemistry of the mono-pyridyl ligands a[10–14] and b,[15] and of the di-pyridyl derivative c.[16,17] 3-(4-Pyridyl)-acetylacetone (Scheme 1, a) has also been employed in halogen- and hydrogen-bonded extended structures.[18] In contrast, the N donor capabilities of the nitrile-substituted

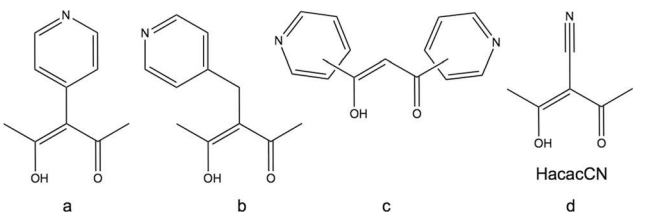

Scheme 1 Examples of ditopic Hacac derivatives.

[a] *Institute of Inorganic Chemistry, RWTH Aachen University, Aachen, Germany. E-mail: ullrich.englert@ac.rwth-aachen.de; Fax: +49 241 8092288; Tel: +49 241 8094666*

[b] *Carleton College, 300 North College Street, Northfield, MN, USA. E-mail: sir@carleton.edu; Tel: +1 612 8021080*

† Electronic supplementary information (ESI) available: Crystallographic information in CIF format, displacement ellipsoid plots for 1–7, powder patterns for 2, 3, 5 and 7, intensity ratio $I(f/t)$ for 2 and 3 over larger temperature ranges, intensity of single reflections in 2, 3 and 4, ^{19}F NMR result of 4 and sequence of slides visualizing the phase transition in 2. CCDC 1005519–1005524 1042065–1042067. For ESI and crystallographic data in CIF or other electronic format see DOI: 10.1039/c5ce00043b

3-cyanoacetylacetone HacacCN (Scheme 1, d) are much less pronounced. Earlier work with this ligand has covered the *O*, *O′* coordination chemistry of Cu, Fe,[19] Cr,[20] Al,[21] and rare earth cations.[22,23] All previous examples with the exception of a Cu–Ag bimetallic ladder structure involve coordination numbers of at least 6 at the cations;[19] no square-planar complexes based on acacCN have been structurally characterized to date, although this coordination mode has been encountered for the unsubstituted parent ligand acac and several of its substitution products.[24–26]

In this contribution, we report the synthesis and characterization of the square-planar complex Pd(acacCN)$_2$, **1**, and its use as a building block for bimetallic extended solids based on Pd(II) and Ag(I) cations. Scheme 2 summarizes our results. Given the linear disposition of the peripheral N donor sites in **1** and the general preference of Ag(I) centers for linear coordination, too, the formation of chain polymers **2–6** is no surprise. The fully reversible and structural phase transition in one of these structure types leads to an unpredicted tunable property, and the 3D network **7** represents a less intuitive way for combining its constituents.

2 Results and discussion

2.1 Description of the crystal structures

The square planar building block Pd(acacCN)$_2$, **1**, has been obtained by reaction of the ligand HacacCN with palladium acetate and an auxiliary base in a mixture of water and methanol applying a rather long reaction time of 16 hours. The building unit is obtained as phase pure yellow microcrystalline powder and can be recrystallized from acetone or THF under formation of yellow needle-shaped crystals.

1 crystallizes in the triclinic space group $P\bar{1}$ with the central palladium cation located on an inversion center. The substituted acetylacetonate deviates only slightly from ideal planarity with the nitrogen atom of the nitrile group 0.034 Å dislocated from the plane defined by palladium and the two coordinating oxygen atoms. For reasons of symmetry, the palladium center and its four coordinating oxygen atoms are exactly coplanar. The coordination environment around the metal features an intra-ligand O–Pd–O bite angle of 94.30(7)° and a *cis* inter-ligand angle of 85.70(7)°. In crystalline **1**, the molecules are arranged in parallel stacks. Each building unit within the stacked layers is displaced by the length of the *a* axis with respect to the next neighboring molecule resulting in close contacts between the carbon atom C3 of each molecule and the Pd atom of the neighboring molecules along the stacking direction. The Pd1^{i}···C3 distance amounts to 3.282(3) Å. Stacking of the molecules and the molecular packing as space filling model is presented in Fig. 1. A similar stacking pattern was described for the unsubstituted Pd(acac)$_2$ complex.[26]

The building block **1** features two uncoordinated nitrile groups with linear NC···Pd···CN arrangement. By addition of silver salts, these weak donor sites may be crosslinked *via* Ag(I) cations to infinite chains. In contrast to the individual constituents, the resulting bimetallic derivatives **2–7** are much less soluble in common solvents and directly precipitate

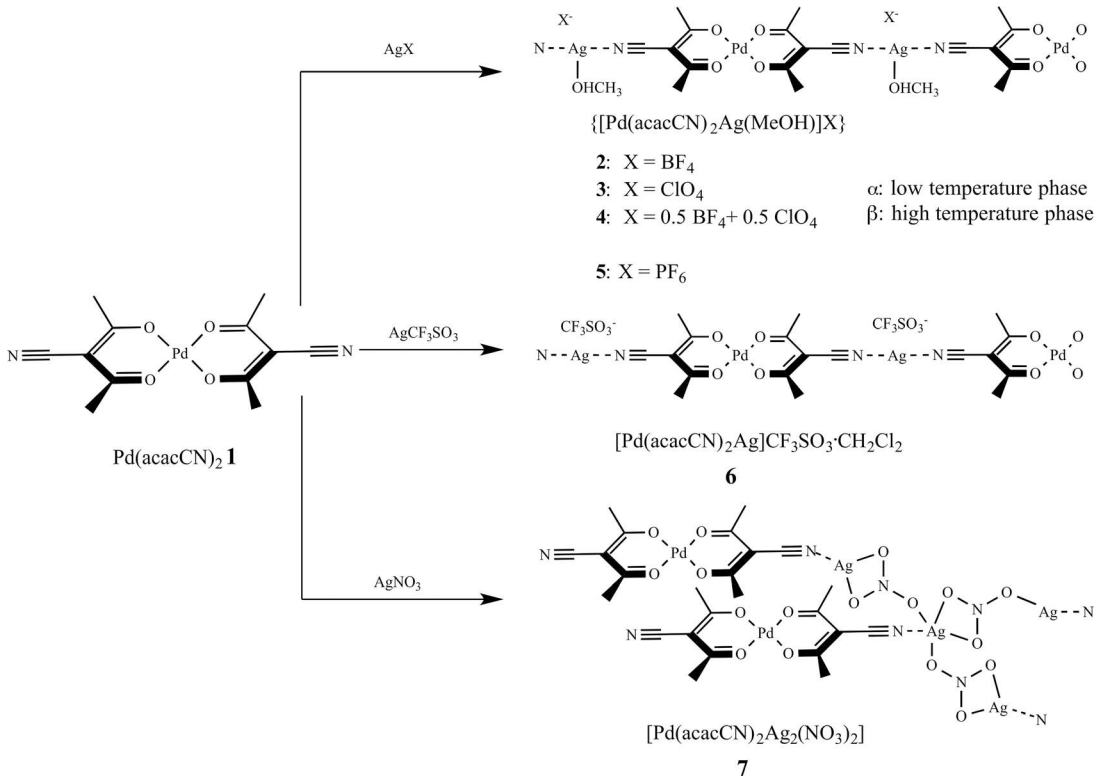

Scheme 2 Synthesis and composition of the building block, **1**; and the bimetallic polymeric solids, **2–7**.

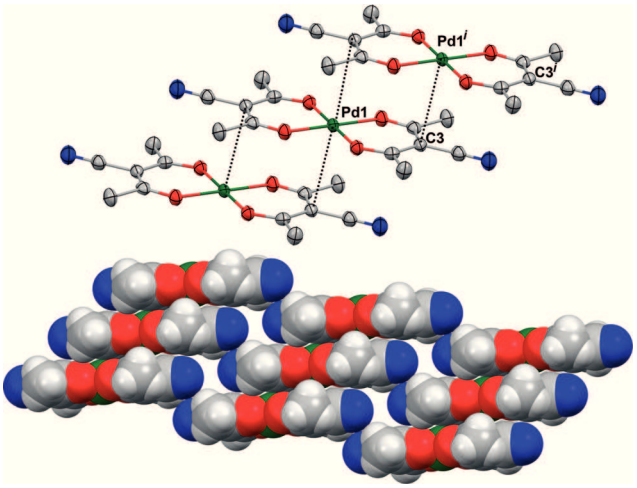

Fig. 1 Intermolecular contacts between Pd1^{i} and C3 within the stacking layers and space filling model of the molecular packing. Ellipsoid are drawn at 75% probability level. Symmetry operation: i = −1 + x, y, z.

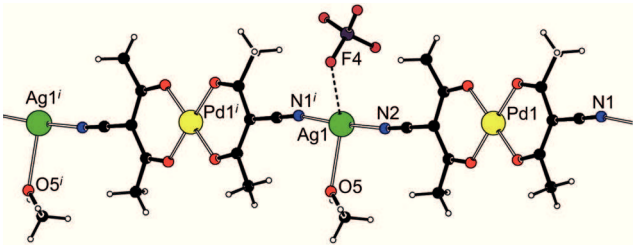

Fig. 2 Section of a polymer chain in **2α** and 2 + 1 + 1 coordination of the Ag(I) cation; the situation in **3α**, **4α** and **5** is similar. Symmetry operator i = x + 1, y, 1 − z.

from solutions of the required stoichiometry. N coordination of a silver ion results in a significant shift in the IR resonance associated with the C–N triple bond to higher wavenumbers.[23] In the chain polymers **2–6**, Pd building blocks and Ag(I) cations are arranged in an alternating sequence, thus forming one-dimensional cationic scaffolds with the counterions included in voids of the crystal structures, in direct neighborhood of the Ag(I). A comparison of intra- and interchain parameters is provided in Table 1.

Compounds **2–5** are methanol solvates. **2** and **3** are isomorphous and show a phase transition at low temperature (see section 2.2, Tunable phase transition); for easier comparison, the following discussion will address the low temperature α phases. In order to study the relationship between chemical composition and phase transition temperature, we prepared the mixed crystal **4**, also isomorphous to **2** and **3**. **5** adopts a crystallographically different but topologically equivalent solvate structure. As an example, a section of the polymer chain in the crystal structure of **2α** is showing Fig. 2. Fig. 2 also shows the Ag(I) environment in the solids **2α–5**: each cation adopts a 2 + 1 + 1 coordination. In addition to its almost linear coordination by two nitrile N atoms in direction of the polymer chain, a significantly longer interaction with a methanol oxygen exists perpendicular to the strand. On the opposite side of the polymer, the counter anion resides; its closest contact to the Ag(I) cation is still within the commonly accepted van der Waals radii. The 4 atoms interacting with the silver cation are almost coplanar. Table 2 summarizes the details concerning Ag(I) coordination.

Chain polymer **6** is a CH_2Cl_2 solvate. Its essentially linear coordinated Ag(I) cations prefers a secondary interaction with the counteranion triflate. This behavior does not only reflect the less pronounced donor capabilities of the solvent but is also in agreement with results from Mak and Chen,[27] who state in a more general context that triflate acts as a more coordinating counteranion than BF_4^-, ClO_4^- or PF_6^-. The asymmetric unit of **6** contains two symmetrically independent Pd(II) cations situated on crystallographic centres of inversion as well as two acacCN ligands, an Ag(I) cation, a triflate anion and a solvent molecule in general position; in line with these symmetry requirements, coordination of the anion to silver occurs from alternating sides of the polymer strand, *cf.* Fig. 3.

Classical hydrogen bonds in **2α–5** only occur along the chains and are entirely absent in **6**. The individual polymer strands in **2α–6** only weakly interact without specific short interchain contacts. Fig. 4 shows the packing in **2α** along the chain direction: stacking of cationic polymers precludes highly efficient space filling. We will come back to this point in the context of the packing discussion of **7**.

2α–5 are moderately stable, **6** rather instable towards desolvation. Larger single crystals may easily be recovered from the mother liquor and handled in air for minutes. Grinding of the samples for powder diffraction results in crystalline solids; their powder patterns, however, do not match the simulation based on the single crystal structures. When solid samples of **2α**, **3α** and **5** are freshly isolated,

Table 1 Comparison of intra- and interchain parameters in **2–6**

Comp.	Chain direction	Pd···Pd (intra, Å)	Ag···Pd···Ag (deg)	Pd···Pd (inter, Å)
2α	[1 0 −1]	15.8275(14)	179.13(2)	4.5849(6)
3α	[1 0 −1]	15.8403(3)	179.40(2)	4.6068(8)
5	[1 −1 −1]	15.790(7)	176.32(2)	4.818(2)
6	[1 0 −1]	15.769(2)	180.0	4.9592(6)

Table 2 Details concerning Ag(I) coordination in **2–5**

Comp.	Ag–N (Å)	N–Ag–N (deg)	Ag···O (methanol, Å)	Ag···X (anion, Å)
2α	2.135(4), 2.135(4)	175.74(13)	2.573(3)	2.716(3) (X = F)
3α	2.134(2), 2.138(2)	178.70(10)	2.598(2)	2.762(2) (X = O)
4α	2.126(5), 2.133(5)	175.5(2)	2.567(5)	2.710(4) (X = 0.5 F + 0.5 O)
5	2.100(7), 2.105(7)	169.8(3)	2.551(9)	2.807(11) (X = F)

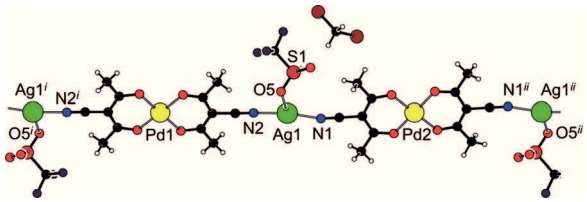

Fig. 3 Section of a polymer chain in **6**; *i* = −1 − *x*, 2 − *y*, 1 − *z*; *ii* = 2 − *x*, 2 − *y*, −1 − *z*.

hardly ground and subjected to powder diffraction while still moist, the powder pattern of the bulk is in agreement with the expectation from the single crystal structure. The corresponding powder patterns for these solids are shown in the ESI† (Fig. S9–S11). The moderately fast desolvation also causes problems in elemental analyses of the bulk; in the case of **5** removal of the solvent seems to be incomplete. In contrast, we have not been able to obtain a powder pattern for **6** which matches its single crystal structure; shortly after removal from the mother liquor, isolated material already corresponds to the solvent-free compound as shown by elemental analysis, *cf.* 4.2.3.

In contrast to the chain polymers discussed above, compound **7** forms a 3D network: neutral layers of the composition $[AgNO_3]_n$ extend in the crystallographic *ac* plane, and $Pd(acacCN)_2$ building blocks oriented along the *b* axis connect these layers in the third dimension as shown in Fig. 5.

The silver coordination in **7** differs significantly from that in the chain polymers: each Ag cation is coordinated by only one acacCN nitrogen atom and by four oxygen atoms of three different nitrate groups. In agreement with the layer stoichiometry, each nitrate coordinates three different cations, one of them in a chelating fashion. The coordination around a cation and that of a nitrate anion are shown in Fig. 6.

The coordination polyhedron around silver may be described as a distorted square pyramid, with N1 at the apex and the oxygen atoms in the basal plane. The distorsion is reflected in the fact that the Addison τ[28] and the Holmes[29] parameter do not agree with respect to the idealized polyhedron: the former amounts to 0.03 and hence almost the ideal value for square-pyramidal coordination whereas the latter indicates 41% of square-pyramidal character on the Berry

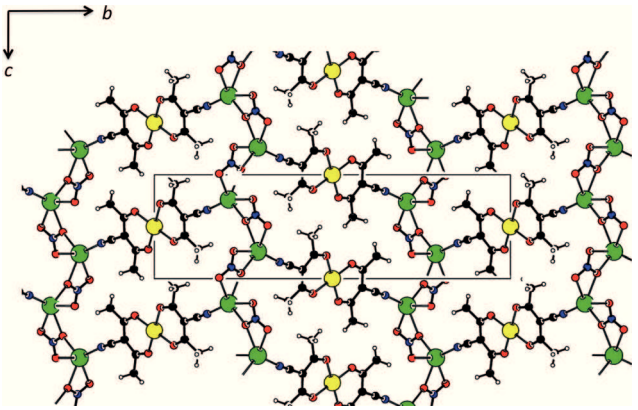

Fig. 5 3D network in the crystal structure of **7**.

pseudo rotation path towards trigonal-bipyramidal coordination. Space filling in **7** (fraction of occupied *versus* total volume[30] 0.747) is more efficient than in the chain polymers **2**–**5** (0.705–0.708) or in the molecular compound **1** (0.716). We also emphasize that our 3D coordination polymer **7** is obtained as a phase pure product: Fig. S12 (in the ESI†) shows the powder pattern of the bulk as synthesized and the calculated pattern based on the single crystal X-ray diffraction experiment. A few examples[31–36] involving nitrate anions which coordinate three Ag cations have been documented in the CSD.[37,38]

2.2 Tunable phase transition

With respect to topology, **2** and **3** are related to the other chain polymers; their structure corresponds to chemical intuition. During bulk characterization of these compounds, we detected discrepancies between their crystal structures at 100 K and room temperature. We will shortly explain the relationship between low- and high temperature phases: according to the symmetry principle,[39] the symmetry relationship between solids before and after a structural phase transition can be described with the help of group theory. For a detailed overview about the concepts in the following discussion, we refer to the excellent monography by Müller.[40] In a second order

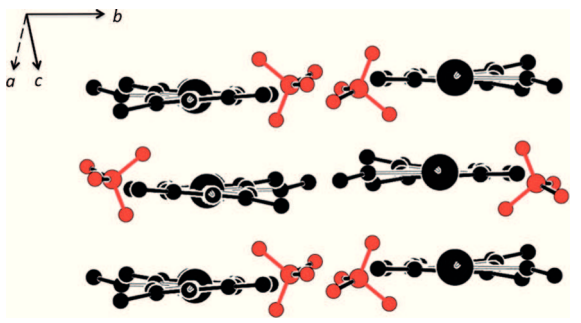

Fig. 4 Projection of **2**α in the direction of the polymer chains, along [1 0 −1]; cationic chains are shown in black, BF_4^- counter anions in red.

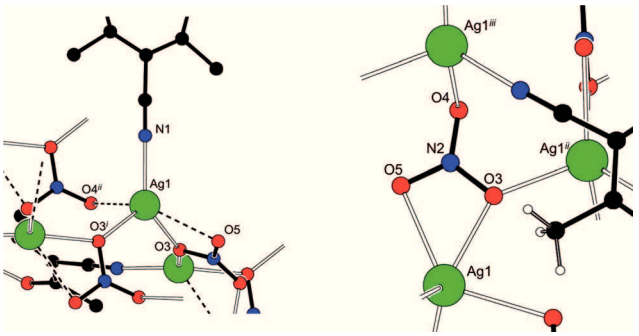

Fig. 6 Coordination of an Ag(I) cation (left) and an anion (right) in the crystal structure of **7**; *i* = 3 − *x*, −*y*, 1 − *z*; *ii* = *x*, 0.5 − *y*, *z* − 0.5; *iii* = *x* − 1, 0.5 − *y*, *z* − 0.5.

phase transition, cooling of a high temperature form results in a phase of lower symmetry. The new phase either adopts a translationengleiche (*t*) or klassengleiche (*k*) subgroup of the original space group. If the phase transition starts from a single crystal, a *t* phase transition will give a twin, with the twin domains related by the symmetry element missing in the subgroup. Twins of this kind are often easy to detect by diffraction experiments. In contrast, a *k* phase transition produces antiphase domains; their diffraction pattern can in general not be distinguished from that of a single crystal. Phase transitions of the *k* type are not readily detected by diffraction; the transition may show up in thermal analysis but the enthalpy associated with a second order phase transition may be small. In the field of molecular crystals, we are aware of earlier work by Guzei *et al.*[41,42] and of a temperature-dependent study concerning tris(acetylacetonato) complexes of aluminium[43] and chromium.[44] We have encountered this situation for the isomorphous chain polymers **2** and **3**; Scheme 3 shows the symmetry relation between their phases.

As **2** and **3** are isomorphous but differ in the phase transition temperature, we also prepared the solid solution **4**. For this compound, the combination of tentative occupancy refinements based on diffraction data (see 4.3) and NMR results (see 4.2.2) suggests statistical disorder of the counter anions BF_4^- and ClO_4^- in equimolar ratio. We can thus correlate the transition temperature with chemical composition. Temperature-dependent powder diffraction, usually the method of choice for monitoring phase transitions, cannot be applied in the present case because loss of the weakly coordinated methanol molecules leads to decomposition and formation of structurally different solvent-free compounds. Fortunately, larger single crystals are much more inert with respect to desolvation and even allow for data collection times of several hours at elevated temperatures, *e.g.* 320 K. Therefore, analysis of the phase transition in each solid required several full intensity data collections in the proximity of its transition temperature; these experiments also unambiguously confirmed that the phase transition is fully reversible. Details are given in the Experimental part.

We will first focus on the effects of the phase transition in real space. In the low temperature α phases, all atoms reside in general position in space group $P2_1/c$, with a complete formula unit of the chain polymer in the asymmetric unit. As an example, the geometry for **2**α is discussed here; the situation in the low temperature forms of **3** and **4** is very similar. The Ag(I) cation is coordinated by two nitrile groups at short distances (*ca.* 2.1 Å) in an almost linear fashion (N1–Ag1–N2i = 175.75(15) Å). Additional interactions involve close contacts to a solvent methanol molecule (Ag1–O5 = 2.573(4) Å) and to a tetrafluoroborate anion (Ag1–F4 = 2.716(3) Å). In the other compounds, perchlorate (**3**) or a mixture of tetrafluoroborate/perchlorate with statistical occupancy (**4**) act as counteranions. Angles involving the longer contact distances, *e.g.* O–Ag–N, show that the overall Ag environment is asymmetric (Fig. 7 bottom).

In the high temperature β phases, the chain polymers adopt space group *C*2/*c* with Pd(II) and Ag(I) on crystallographic twofold axes. Consequently, the asymmetric unit comprises only half a formula unit of the polymer. The resulting local environment about Ag(I) (Fig. 7 top) exhibits very similar values for the short Ag–N distances and the subtended angle as in the α phase. It is, however, necessarily symmetric, and the metal cations are precisely aligned when viewed in the direction of chain propagation, *i.e.* along [1 0 −1]. Symmetry in the β phases involves disorder of the coordinated methanol molecules about the crystallographic twofold axis passing through the Ag(I) center.

How about reciprocal space? The C centering of the unit cells associated with the high temperature β forms implies the integral reflection condition *hkl*, $h + k = 2n$. Reflection intensities for *hlk*, $h + k = 2n + 1$ should be systematically

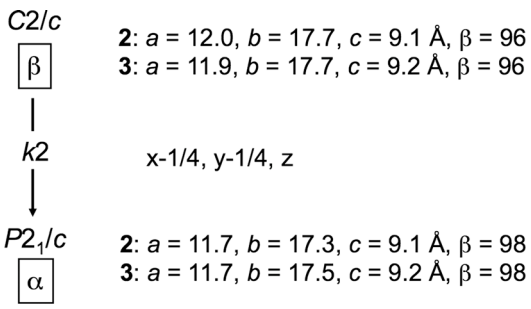

Scheme 3 Symmetry relationship between the high (b) and low (a) temperature phases of the compounds.

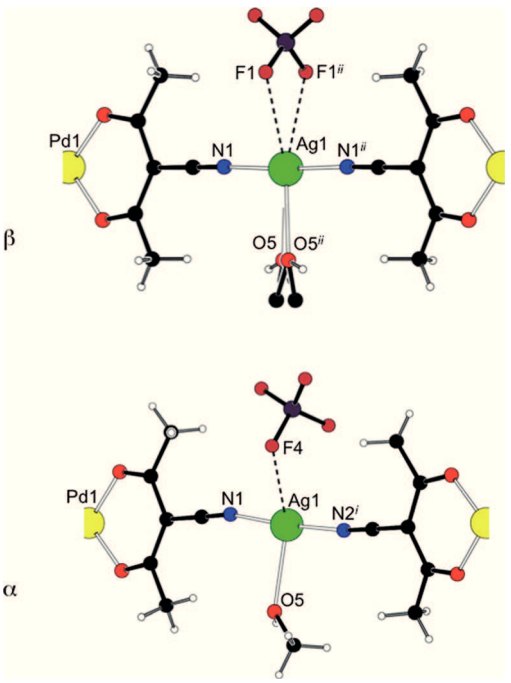

Fig. 7 Local environment about the Ag(I) cations in the β (top) and α (bottom) phase of **2**; view direction is along [0 0 1]. The situation for **3** and **4** is similar. Symmetry operators: *i* = *x* + 1, *y*, *z* − 1; *ii* = 2 − *x*, *y*, 0.5 − *z*.

absent. With respect to the overall diffraction pattern, the ratio between the latter forbidden and the former allowed reflection intensities, expressed as

$$I(f/t) = \frac{\sum I_{(h+k=2n+1)}}{\sum I_{(h+k=2n)}} \quad (1)$$

should assume very small values, ideally zero, at the phase transition temperature. The *ab* plane with its C centering for the high temperature phases is shown in Fig. 8a.

For the low temperature α phases, no integral reflection condition can be expected. Fig. 8b shows, however, that the arrangement of the most relevant scattering centers in the α phases is rather similar to that in β: pronounced pseudo-symmetry is observed, and therefore the intensity of reflections *hkl*, $h + k = 2n$ exceed those of *hlk*, $h + k = 2n + 1$ significantly, even below the phase transition temperature. This fact was indeed the original motivation for temperature-dependent diffraction experiments on crystals of **2** which ultimately led to the discovery of the phase transition. Even at 100 K, far away from the phase transition temperature, reflections with $h + k = 2n$ are much stronger than those not matching this condition, and hence the corresponding value for $I(f/t)$ in eqn (1) amounts to *ca.* 0.5. Obviously, for any structure without pseudosymmetry, a ratio close to unity is expected. In agreement with the requirements for the order parameter[40] in a second order phase transition, the intensity ratio $I(f/t)$ calculated according to eqn (1) is a function of temperature in the low symmetry form; it approaches a small value at the phase transition and remains close to zero in the high symmetry phase. Remarkably, the isomorphous solids **2** and **3** differ significantly in their phase transition temperatures; Scheme 4 summarizes these results.

Due to relatively fast desolvation of powder samples, our experiments have been conducted on larger and more stable single crystals. Each individual data point specifies an $I(f/t)$ ratio at a given temperature and is based on a complete set of intensity data. In the context of these experiments, we did not only obtain information concerning the transition temperatures but we could also confirm the expectation that the phase transitions are fully reversible and that single crystals can survive even after five consecutive cycles of heating and cooling.

2 and **3** share the same cationic chain polymer structure but differ with respect to their counter anions. The difference in their phase transition temperatures encouraged us to test whether this property might be tuned by chemical substitution in the anionic part of the structure. We had encountered an analogous example for the t_2 phase transition in the one-dimensional polymers $[Cd(\mu\text{-}X)_2py_2]$ (X = Cl, Br; py = pyridine).[1] A chain polymers in which tetrafluoroborate and perchlorate occupy the anion positions in statistical distribution can indeed be prepared: this molecular alloy **4** is also isomorphous with **2** and **3**, crystallizing in the same space group with similar lattice parameters. Tentative refinement of the atomic site occupancies in the anion region unambiguously proved the concomitant presence of tetrafluoroborate and perchlorate. In the final refinement of the low temperature intensity data for **4α**, the anion site was treated as equally populated by both alternative anions; additional details are provided in section 4. Coordination polymer **4** also meets the

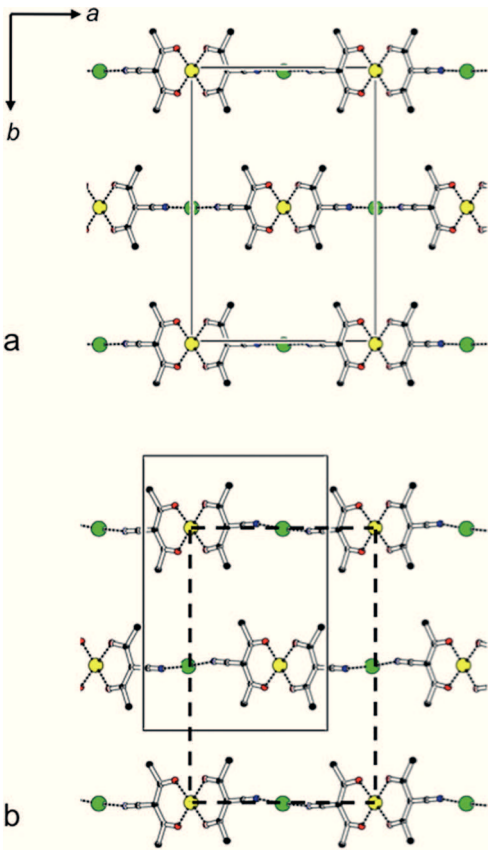

Fig. 8 Projections of the C-centered β phase (a) and the pseudo-centered α phase (b) of **2**; conventional unit cells are indicated by solid, the centered pseudo-cell for **2α** by dashed lines. H atoms, coordinated methanol and BF_4^- anions have been omitted for clarity; the situation in **3** and **4** is similar.

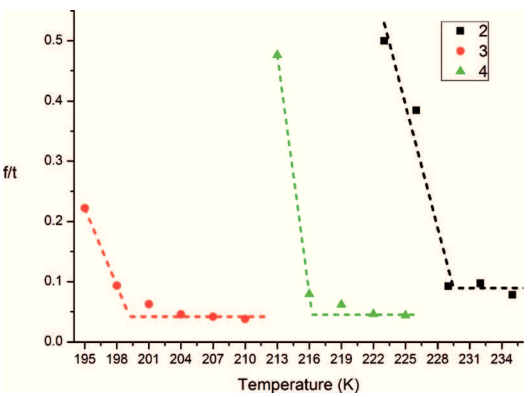

Scheme 4 Intensity ratio $I(f/t)$ as a function of temperature for **2**, **3** and the mixed anion compound **4**.

expected property with respect to the k_2 phase transition and features an intermediate transition temperature as shown in Scheme 4. In view of the fact that intensity data collected at 320 K, *i.e.* well above the phase transition temperatures, showed large anisotropic displacement parameters for the individual anions in **2** and **3**, no attempt was made to establish a disorder model with atomic resolution for the high temperature form **4β**.

3 Conclusion

Crosslinking of the new building block Pd(acacCN)$_2$, **1**, with silver salts leads to products of two topologies. In **2–6**, the alternating arrangement of neutral Pd(acacCN)$_2$ units and Ag(I) cations results in cationic chains, with counteranions and solvent molecules close to the silver. In the alternative 3D network **7**, Pd(acacCN)$_2$ bridges $[AgNO_3]_n$ layers. In contrast to the less coordinating anions BF_4^- or PF_6^-, nitrate is well-known to coordinate to Ag(I): both chelating and bridging geometries occur with quite high frequency. A search in the Cambridge Structural Database[37,45] revealed 721 entries in which a nitrate anion is coordinated to silver. In 274 of these cases, a chelating NO_3 coordination to Ag was observed, and in 261 entries a nitrate was found bridging between at least two silver centers. 120 crystal structures combine both chelating and bridging nitrate moieties. Future work will be devoted to synthesize and understand more structures featuring $AgNO_3$ layers.

Our interest is not limited to static crystal structures: the chain polymers **2–4** provide a beautiful example for a k_2 phase transition which may be tuned by chemical substitution. Furthermore, they convey a more general message: a solid studied in a routine diffraction experiment at a single (low) temperature may well be the result of an undetected *k* phase transition. In the case of **2**, pseudosymmetry has been the key indicator which stimulated additional diffraction experiments at variable temperature, and pseudo symmetry may readily be detected. Pseudosymmetric structures may be retrieved in real space, *e.g.* by screening 3D coordinates available from data bases, or in reciprocal space, by comparing the intensities for different classes of reflections. Our future work will focus on the former approach.

4 Experimental part

4.1 Materials and methods

The HacacCN ligand was prepared according to the literature method by Silvernail *et al.*[46] All chemicals were used without further purification: palladium acetate (Acros Organics), $NaHCO_3$ (99.5%, KMF Laborchemie), NaF (99%), NaI (AppliChem), D_2O (99.9%, Aldrich), $AgPF_6$ (98%, Aldrich), $AgCF_3SO_3$ (98%, Acros Organics), $AgClO_4$ (Alfa Aesar), $AgBF_4$ (98%, Aldrich), and $AgNO_3$ (99.5%, Fluka Chemie).

IR spectra were recorded on a Nicolet Avatar 360 E.S.P. spectrometer in KBr windows for **1** and in nujol mull for **2**, **3**, **5** and **7**. CHN microanalyses were carried out at the Institute of Organic Chemistry, RWTH Aachen University, using a HERAEUS CHNO-Rapid. Powder diffraction experiments were performed at room temperature on flat samples with a Stoe & Cie STADI P diffractometer equipped with an image plate detector with constant ω angle of 55° using germanium-monochromated Cu-$K_{\alpha1}$ radiation (λ = 1.54051 Å).

4.2 Syntheses

4.2.1. Synthesis of Pd(acacCN)$_2$, 1. HacacCN (250 mg, 2 mmol) was dissolved in a mixture of MeOH/H_2O (2 mL/7 mL). $NaHCO_2$ (168 mg, 2 mmol) was slowly added (20 min). Palladium acetate (224 mg, 1 mmol) was suspended in the solution of the deprotonated ligand. The suspension was stirred for 16 hours at 35 °C. After two hours formation of a yellow solid started. After sixteen hours the yellow precipitate was filtered (G3 frit with pore size of *ca.* 20–40 microns), washed with water, and dried in a desiccator. Yield: 253 mg (0.71 mmol, 71%). Recrystallization from acetone allowed the growth of suitable single crystals. Analysis: CHN: anal. calcd. for [Pd(acacCN)$_2$]: $C_{12}H_{12}PdN_2O_4$: C: 40.64, H: 3.41, N: 7.90. Found: C: 40.32, H: 3.38, N: 7.85. IR: ν(C≡N, cm^{-1}) = 2210.

4.2.2 Syntheses of [Pd(acacCN)$_2$Ag(MeOH)]BF$_4$, 2, [Pd(acacCN)$_2$Ag(MeOH)]ClO$_4$, 3, [Pd(acacCN)$_2$Ag(MeOH)]0.5BF$_4$·0.5ClO$_4$, 4 and [Pd(acacCN)$_2$Ag(MeOH)]PF$_6$, 5. The building unit **1**, (18 mg, 0.05 mmol) was dissolved in 3 mL CH_2Cl_2. $AgBF_4$ (9 mg, 0.05 mmol) was dissolved in 3 mL methanol and layered above it with an intermediate layer of 1 mL CH_2Cl_2 and 1 mL methanol. Yellow crystals were obtained after one week of crystallization time and single crystal X-ray diffraction characterized them as the linear chain polymer **2α**. Yield: 14 mg (0.025 mmol, 50%) Analysis: CHN: anal. calcd. for [Pd(acacCN)$_2$AgBF$_4$]: $C_{12}H_{12}AgBF_4N_2O_4Pd$: C: 26.24, H: 2.20, N: 5.10. Found: C: 26.16, H: 2.70, N: 4.76. IR: ν(C≡N, cm^{-1}) = 2237.

The analogous reaction conducted with $AgClO_4$ (10 mg, 0.05 mmol) and $AgPF_6$ (13 mg, 0.05 mmol) as cross-linking reagent yielded the chain polymers **3** and **5**, respectively. Yield for **3**: 15 mg (0.027 mmol, 54%) Analysis: CHN: anal. calcd. [Pd(acacCN)$_2$AgClO$_4$]: $C_{12}H_{12}AgClN_2O_8Pd$: C: 25.65, H: 2.15, N: 4.98. Found: C: 25.87, H: 2.47, N: 4.80. IR: ν(C≡N, cm^{-1}) = 2229. Yield for **5**: 16 mg (0.026 mmol, 52%) Analysis: CHN: anal. calcd. for [Pd(acacCN)$_2$AgPF$_6$]: $C_{12}H_{12}AgF_6N_2O_4PPd$: C: 23.72, H: 1.99, N: 4.61. Found: C: 24.54, H: 2.41, N: 4.55. IR: ν(C≡N, cm^{-1}) = 2237.

For the more complex case of the mixed crystals **4**, in a test tube, the building block Pd(acacCN)$_2$ (0.018 g, 0.05 mmol) was dissolved in 3 mL CH_2Cl_2. A solvent mixture of 0.10 mL CH_2Cl_2 and 0.10 mL CH_2OH was used as an intermediate layer, and a solution of $AgBF_4$ (0.008 g, 0.04 mmol) and $AgClO_4$ (0.002 g, 0.01 mmol) in 1 mL CH_3OH was layered on top. After 2 days, yellow crystals of **4** were obtained. The composition of these mixed crystals with respect to the anion content was determined by site occupancy refinement (see section 4.3) and controlled by ^{19}F NMR spectroscopy. For this purpose, a known quantity of **4** was decomposed by addition of NaI in D_2O; after separation from the precipitated AgI, a solution of NaF in D_2O

was added as internal standard. Integration of the ^{19}F resonances suggested a BF_4^- content of *ca.* 0.4 per Ag(I) cation.

Single crystals of **2–5** are stable for a limited amount of time after they have been removed from the reaction mixture. Grinding of the products for powder diffraction studies showed rapid loss of the coordinated methanol molecules for all three structures. Therefore all yield calculations and theoretical CHN values refer to the solvent free compounds.

4.2.3 Synthesis of $[Pd(acacCN)_2Ag]CF_3SO_3{\cdot}CH_2Cl_2$, 6. The building unit **1**, (18 mg, 0.05 mmol) was dissolved in 3 mL CH_2Cl_2. $AgCF_3SO_3$ (13 mg, 0.05 mmol) was dissolved in 3 mL of methanol and layered on top of an intermediate layer of 2 mL CH_2Cl_2 Yellow crystals were obtained after one week of crystallization time and single crystal X-ray diffraction characterized them as the linear chain polymer **6**. Crystals lose their crystallinity within minutes when they are removed from the reaction mixture. For CHN analysis and yield calculation crystals were dried in vacuum, and calculated values refer to the solvent free compound. Yield: 18 mg (0.029 mmol, 58%) Analysis: CHN: anal. calcd. for $[Pd(acacCN)_2AgCF_3SO_3]$: $C_{13}H_{12}AgF_3N_2O_7PdS$: C: 25.53, H: 1.98, N: 4.58. Found: C: 24.89, H: 2.13, N: 4.04.

4.2.4 Synthesis of $[Pd(acacCN)_2Ag_2(NO_3)_2]$, 7. The building unit **1**, (18 mg, 0.05 mmol) was dissolved in 3 mL CH_2Cl_2. $AgNO_3$ (16 mg, 0.10 mmol) was dissolved firstly in one drop of water and then 3 mL of methanol were added. The solution was layered on top of the building unit solution with an intermediate layer of 1 mL CH_3Cl_3 and 1 mL methanol. Yellow crystals were obtained after one day of crystallization time and they were identified by single crystal X-ray diffraction as 3D network **7**. Crystals are stable after they have been removed from the reaction mixture. Yield: 19 mg (0.028 mmol, 56%) Analysis: CHN: anal. calcd. for $[Pd(acacCN)_3Ag_2(NO_3)_2]$: $C_{12}H_{12}Ag_2N_4O_{10}Pd$: C: 20.76, H: 1.74, N: 8.07. Found: C: 20.73, H: 1.80, N: 8.08. IR: ν(CN, cm^{-1}) = 2233.

4.3 Crystallographic studies

The diffraction experiments (Tables 3–5) were performed with a Bruker D8 goniometer equipped with an Incoatec microsource (Mo-K_α, λ = 0.71073 Å, multilayer optics) and an APEX CCD detector; the sample temperature was controlled with an accuracy of *ca.* 2 K with an Oxford Cryostream 700 instrument. Intensity data were integrated with *SAINT+* [47] and corrected for absorption by multi-scan methods using the program SADABS.[48]

Details about the structure models are given at the end of this section; we first describe the temperature-dependent diffraction experiments for establishing the phase transition temperatures. Powder diffraction would usually be the method of choice and much faster; powder samples of the coordination polymers **2–4**, however, undergo fast desolvation of co-crystallized methanol, and reliable powder patterns can only be obtained on moist samples for a short period. All diffraction data have therefore been collected on single crystals which proved considerably more stable towards solvent evaporation. For each compound, a subset of intensity data was collected at intervals of 15 K to roughly determine the transition temperature. Close to the phase transition, complete

Table 3 Crystal data and refinement results for the square planar building unit $Pd(acacCN)_2$, **1**, and the bimetallic coordination polymers **2** at 100 K and 320 K

Compound	**1**	**2α**	**2β**
Temperature (K)	100(2)	100(2)	320(2)
Empirical formula	$C_{12}H_{12}N_2O_4Pd$	$C_{13}H_{16}AgBF_4N_2O_5Pd$	$C_{13}H_{16}AgBF_4N_2O_5Pd$
Moiety formula	$C_{12}H_{12}N_2O_4Pd$	$C_{12}H_{12}AgN_2O_4Pd$, BF_4, CH_3OH	$C_{12}H_{12}AgN_2O_4Pd$, BF_4, CH_3OH
Formula weight (g mol^{-1})	354.64	581.37	581.37
Crystal description	Yellow plate	Yellow plate	Yellow plate
Crystal size (mm)	0.35 × 0.11 × 0.09	0.24 × 0.20 × 0.16	0.26 × 0.22 × 0.26
Crystal system	Triclinic	Monoclinic	Monoclinic
Space group	$P\bar{1}$	$P2_1/c$	$C2/c$
a (Å)	4.8536(11)	11.6947(9)	11.9640(16)
b (Å)	7.8906(17)	17.3278(14)	17.688(2)
c (Å)	8.8251(19)	9.1324(7)	9.1080(11)
α (°)	78.1348(27)		
β (°)	86.3966(28)	98.1670(11)	96.437(3)
γ (°)	75.1220(28)		
V (Å^3)	319.65(12)	1831.9(2)	1915.3(4)
Z	1	4	4
μ (mm^{-1})	1.462	2.117	2.025
Total/unique reflections	4614/1768	21 198/3820	5071/1747
R_{int}	0.0401	0.0597	0.0245
$R[F^2 > 2\sigma(F^2)]$	0.0282	0.0418	0.0322
wR_2 (F^2)	0.0670	0.1242	0.1291
GOF	1.091	1.132	1.000
No. of parameters	90	253	137
$\Delta\rho_{max}/\Delta\rho_{min}$ (e Å^{-3})	0.673/−0.708	1.171[a] /−1.224[b]	0.411/−0.515
CCDC	1005519	1005520	1042065

[a] Highest peak 1.171 is 1.29 Å from *F*2. [b] Deepest hole − 1.22 is 0.75 Å from Pd1.

Table 4 Crystal data and refinement results for **3** at 100 K and 320 K as well as **4** at 100 K

Compound	3α	3β	4α
Temperature (K)	100(2)	320(2)	100(2)
Empirical formula	$C_{13}H_{16}AgClN_2O_9Pd$	$C_{13}H_{16}AgClN_2O_9Pd$	$C_{13}H_{16}AgB_{0.5}Cl_{0.5}F_2N_2O_7Pd$
Moiety formula	$C_{12}H_{12}AgN_2O_4Pd$, ClO_4, CH_3OH	$C_{12}H_{12}AgN_2O_4Pd$, ClO_4, CH_3OH	$C_{12}H_{12}Ag_2N_2O_4Pd$, $0.5BF_4$, $0.5ClO_4$, CH_3OH
Formula weight (g mol^{-1})	594.02	594.02	587.68
Crystal description	Yellow plate	Yellow prism	Yellow rod
Crystal size (mm)	0.19 × 0.15 × 0.09	0.60 × 0.23 × 0.14	0.29 × 0.17 × 0.17
Crystal system	Monoclinic	Monoclinic	Monoclinic
Space group	$P2_1/c$	$C2/c$	$P2_1/c$
a (Å)	11.7013(18)	11.9150(17)	11.6840(11)
b (Å)	17.518(3)	17.722(3)	17.2956(16)
c (Å)	9.1703(14)	9.1692(13)	9.1223(9)
β (°)	98.006(2)	96.440(2)	98.158(2)
V (Å^3)	1861.4(5)	1924.0(5)	1824.8(3)
Z	4	4	4
μ (mm^{-1})	2.211	2.139	2.190
Total/unique reflections	22 129/3852	10 680/1794	19 702/3294
R_{int}	0.0450	0.0508	0.0423
$R[F^2 > 2\sigma(F^2)]$	0.0250	0.0359	0.0412
wR_2 (F^2)	0.0657	0.1194	0.1063
GOF	1.033	0.986	1.060
No. of parameters	272	137	250
$\Delta\rho_{max}/\Delta\rho_{min}$ (e Å^{-3})	0.759/−0.667	0.659/−1.189[a]	2.432[b] /−1.105[c]
CCDC	1005521	1042066	1042067

[a] Deepest hole − 1.189 is 0.74 Å from Ag1. [b] Highest peak 2.432 is 0.87 Å from Pd1. [c] Deepest hole − 1.105 is 0.53 Å from Cl1.

Table 5 Crystal data and refinement results of the bimetallic coordination polymers **5**, **6**, and **7**

Compound	5	6	7
Temperature (K)	100(2)	100(2)	100(2)
Empirical formula	$C_{13}H_{16}AgF_6N_2O_5PPd$	$C_{14}H_{14}AgCl_2F_3N_2O_7PdS$	$C_{12}H_{12}Ag_2N_4O_{10}Pd$
Moiety formula	$C_{12}H_{12}AgN_{12}O_{12}Pd$, PF_6, CH_3OH	$C_{12}H_{12}AgN_2O_4Pd$, CF_3SO_3, CH_2Cl_2	$C_{12}H_{12}Ag_2N_2O_4Pd$, 2 NO_3
Formula weight (g mol^{-1})	639.53	696.50	694.40
Crystal description	Yellow plate	Yellow prism	Yellow rod
Crystal size (mm)	0.29 × 0.17 × 0.10	0.14 × 0.10 × 0.04	0.11 × 0.05 × 0.04
Crystal system	Triclinic	Triclinic	Monoclinic
Space group	$P\bar{1}$	$P\bar{1}$	$P2_1/c$
a (Å)	9.358(4)	9.9183(13)	4.6283(8)
b (Å)	10.882(5)	10.7825(14)	25.815(4)
c (Å)	10.968(4)	11.6604(15)	7.8121
α (°)	116.299(6)	65.896(2)	
β (°)	96.468(6)	71.7491(19)	105.265(2)
γ (°)	91.599(6)	88.957(2)	
V (Å^3)	991.2(7)	1072.3(2)	900.5(3)
Z	2	2	2
μ (mm^{-1})	2.058	2.163	3.205
Total/unique reflections	7996/3479	15 506/5733	10 789/1878
R_{int}	0.0447	0.0443	0.0323
$R[F^2 > 2\sigma(F^2)]$	0.0592	0.0374	0.0180
wR_2 (F^2)	0.1765	0.0838	0.0440
GOF	1.091	0.992	1.071
No. of parameters	268	287	135
$\Delta\rho_{max}/\Delta\rho_{min}$ (e Å^{-3})	2.544[a] /−1.648[b]	0.912/−0.857	0.445/−0.556
CCDC	1005522	1005523	1005524

[a] Highest peak 2.544 is 0.97 Å from Pd1. [b] Deepest hole − 1.648 is 0.94 Å from Pd1.

intensity data sets were collected according to nested intervals above and below the transition temperature in 3 K steps. In this way, the phase transition temperature could be determined with reasonable accuracy and at the same time the reversibility of the transition could be proven.

The crystal structures were solved with Patterson or Direct methods, and refinements were accomplished with full matrix least-square procedures as implemented in SHELXL-13.[49] All non-hydrogen atoms were assigned anisotropic displacement parameters; hydrogen atoms were placed in idealized positions

and included as riding with constrained isotropic displacement parameters. In **2**, **3**, **4** and **5**, the hydrogen atoms of the hydroxyl group of the methanol molecule were located as electron density maxima from the Fourier difference maps and included in the refinement with distance restraints.

For compounds **2**–**4**, the data collection temperatures of 100 and 320 K were well below or above the phase transitions temperatures, and assignment of the space groups was unambiguous. In **3α**, two oxygen atoms of the perchlorate anion showed positional disorder. The occupancy of two alternative positions was refined using distance restraints; it converged at a 40 : 60 ratio for the alternative orientations. In the case of **4**, tentative refinements allowed to exclude simple BF_4^- or ClO_4^- models for the anion; treatment of this site as substitutionally disordered by both moieties, with constrained coordinates and anisotropic displacement parameters, suggested a slight (60 : 40) preference of tetrafluoroborate over perchlorate. In view of the correlation between displacement parameters and site occupancies and the potential bias introduced by constraining F (in BF_4^-) and O (in ClO_4^-) to the same coordinates, we undertook an independent analysis based on integration of the ^{19}F NMR resonances (see above). This experiment confirmed the almost equimolar presence of both anion species but rather suggested a slightly preferential occupancy of the anion site by perchlorate. In the final structure model for **4α**, the anion as therefore treated as disordered with equal occupancy for tetrafluoroborate and perchlorate, in reasonable agreement with the results of both experimental methods. No attempt was made to obtain a structure model at atomic resolution for the (necessarily disordered) β phase of **4** under these conditions. After refinement of the structure model for **5**, the most disagreeable reflections showed a clear tendency for F^2(obs.) $\gg$ F^2(calc.). A test with the help of the TwinRotMat option in PLATON[30] confirmed non-merohedral twinning for this sample, with 1056 out of 7996 reflections overlapping. An appropriately modified set of intensity data taking the partially overlapped diffraction of both domains into account (HKLF5 format in SHELXL97[50]) gave significantly improved convergence results and relative domain fractions of 0.75 and 0.25. One fluorine atom of the PF_6^- anion showed positional disorder and the occupancy of two alternative positions was refined converging at a 40 : 60 ratio. The affected atoms were refined with isotropic displacement parameters.

Acknowledgements

Financial support by China Scholarship Council (Q. G.), DFG (SeleCa) and RWTH Graduiertenförderung (C. M.) are gratefully acknowledged. Paul Müller is gratefully acknowledged for help with powder diffraction experiments.

References

1 K. Lamberts, I. Kalf, A. Ramadan, P. Müller, R. Dronskowski and U. Englert, *Polymers*, 2011, **3**, 1151–1161.
2 C. Wang, D. Liu and W. Lin, *J. Am. Chem. Soc.*, 2013, **135**, 13222–13234.
3 L. L. Welbes and A. S. Borovik, *Acc. Chem. Res.*, 2005, **38**, 765–774.
4 D. Banerjee and J. B. Parise, *Cryst. Growth Des.*, 2011, **11**, 4704–4720.
5 H. Furukawa, K. E. Cordova, M. O'Keeffe and O. M. Yaghi, *Science*, 2013, **341**, 974.
6 K. Kishida, S. Horike, Y. Watanabe, M. Tahara, Y. Inubushi and S. Kitagawa, *Chem. – Asian J.*, 2014, **9**, 1643–1647.
7 M.-D. Zhang, H.-G. Zheng, Z.-Z. liu and X.-Q. Yao, *CrystEngComm*, 2013, **15**, 9265–9275.
8 A. Nafady, A. P. O'Mullane and A. M. Bond, *Coord. Chem. Rev.*, 2014, **268**, 101–142.
9 R. G. Pearson, *Chemical Hardness, Applications from Molecules to Solids*, Wiley-VCH, Weinheim, 1997.
10 V. D. Vreshch, A. N. Chernega, J. A. K. Howard, J. Sieler and K. V. Domasevitch, *Dalton Trans.*, 2003, 1707–1711.
11 V. D. Vreshch, A. B. Lysenko, A. N. Chernega, J. A. K. Howard, H. Krautscheid, J. Sieler and K. V. Domasevitch, *Dalton Trans.*, 2004, 2899–2903.
12 C. Merkens, K. N. Truong and U. Englert, *Acta Crystallogr., Sect. B: Struct. Sci., Cryst. Eng. Mater.*, 2014, **70**, 705–713.
13 B. Chen, F. R. Fronczek and A. W. Maverick, *Inorg. Chem.*, 2004, **43**, 8209–8211.
14 Y. Zhang, B. Chen, F. R. Fronczek and A. W. Maverick, *Inorg. Chem.*, 2008, **47**, 4433–4435.
15 D. Simond, S. E. Clifford, A. F. Vieira, C. Besnard and A. F. Williams, *RSC Adv.*, 2014, **4**, 16686–16693.
16 A. D. Burrows, C. G. Frost, M. F. Mahon, P. R. Raithby, C. L. Renouf, C. Richardson and A. J. Stevenson, *Chem. Commun.*, 2010, **46**, 5067–5069.
17 A. D. Burrows, M. F. Mahon, C. L. Renouf, C. R. Richardson, A. J. Warren and J. E. Warren, *Dalton Trans.*, 2012, **41**, 4153–4163.
18 C. Merkens, F. Pan and U. Englert, *CrystEngComm*, 2013, **15**, 8153–8158.
19 A. D. Burrows, K. Cassar, M. F. Mahon and J. E. Warren, *Dalton Trans.*, 2007, 2499–2509.
20 M. Kondracka and U. Englert, *Inorg. Chem.*, 2008, **47**, 10246–10257.
21 C. Merkens, N. Becker, K. Lamberts and U. Englert, *Dalton Trans.*, 2012, **41**, 8594–8599.
22 C. Merkens and U. Englert, *Dalton Trans.*, 2012, **41**, 4664–4673.
23 C. Merkens, O. Pecher, F. Steuber, S. Eisenhut, A. Görne, F. Haarmann and U. Englert, *Z. Anorg. Allg. Chem.*, 2013, **639**, 340–346.
24 D. M. Többens, M. Hummel, R. Kaindl, H. Schottenberger and V. Kahlenberg, *CrystEngComm*, 2008, **10**, 327–334.
25 M. A. G. Berg, M. K. Ritchie and J. S. Merola, *Polyhedron*, 2012, **38**, 126–130.
26 M. Hamid, M. Zeller, A. D. Hunter, M. Mazhara and A. A. Tahira, *Acta Crystallogr., Sect. E: Struct. Rep. Online*, 2005, **61**, m2181–m2183.
27 X.-D. Chen and T. C. W. Mak, *Chem. Commun.*, 2005, 3529–3531.

28 A. W. Addison, T. N. Rao, J. Reedijk, J. van Rijn and G. C. Verschoor, *J. Chem. Soc., Dalton Trans.*, 1984, 1349–1356.
29 R. Holmes, *Inorg. Chem.*, 1984, **32**, 119–235.
30 A. L. Spek, *Acta Crystallogr., Sect. D: Biol. Crystallogr.*, 2009, **65**, 148–155.
31 S.-L. Kuang, H.-Y. Li, D.-B. Dang and X.-J. Pan, *Synth. React. Inorg., Met.-Org., Nano-Met. Chem.*, 2012, **42**, 5964.
32 T. R. Sarangarajan, B. S. Krishnamoorthy, K. Panchanatheswaran, J. N. Low and C. Glidewell, *Acta Crystallogr., Sect. C: Cryst. Struct. Commun.*, 2008, **64**, m286–m291.
33 H. S. Huh, S. Y. Yun and S. W. Lee, *Bull. Korean Chem. Soc.*, 2008, **29**, 1065–1068.
34 H. S. Huh, S. H. Kim, S. Y. Yun and S. W. Lee, *Polyhedron*, 2008, **27**, 1229–1237.
35 Z.-P. Deng, Z.-B. Zhu, S. Gao, L.-H. Huo, H. Zhao and S. W. Ng, *Dalton Trans.*, 2009, 6552–6561.
36 M. H. Shu, C. L. Tu, W. D. Xu, H. B. Jin and J. Sun, *Cryst. Growth Des.*, 2006, **6**, 1890–1896.
37 F. H. Allen, *Acta Crystallogr., Sect. B: Struct. Sci.*, 2002, **58**, 380–388.
38 *CSD version 5.35*, November 2013, with 658007 entries.
39 H. Bärnighausen, *MATCH*, 1980, **9**, 139–175.
40 U. Müller, *Symmetriebeziehungen zwischen verwandten Kristallstrukturen*, Vieweg+Teubner, 2011.
41 I. A. Guzei, L. C. Spencer, J. W. Su and R. R. Burnette, *Acta Crystallogr., Sect. B: Struct. Sci.*, 2007, **63**, 93–100.
42 I. A. Guzei, E. M. Gunn, L. C. Spencer, J. M. Schomaker and J. W. Rigoli, *CrystEngComm*, 2011, **13**, 3444–3450.
43 L. S. von Chrzanowski, M. Lutz and A. L. Spek, *Acta Crystallogr., Sect. C: Cryst. Struct. Commun.*, 2007, **63**, m129–m134.
44 L. S. von Chrzanowski, M. Lutz and A. L. Spek, *Acta Crystallogr., Sect. C: Cryst. Struct. Commun.*, 2007, **63**, m377–m382.
45 All numbers in the following analysis refer to error-free structures without disorder.
46 C. M. Silvernail, G. Yap, R. D. Sommer, A. L. Rheingold, V. W. Day and J. A. Belot, *Polyhedron*, 2001, **20**, 3113–3117.
47 *SAINT+ (version 7.68). Program for reduction of data collected on Bruker CCD area detector diffractometer*, 2009.
48 G. M. Sheldrick, *SADABS (version 2.03). Program for empirical absorption correction of area detector data*, 2004.
49 G. M. Sheldrick, *Acta Crystallogr., Sect. C: Struct. Chem.*, 2015, **71**, 3–8.
50 G. M. Sheldrick, *Acta Crystallogr., Sect. A: Found. Crystallogr.*, 2008, **64**, 112–122.